GEOPHYSICAL RESEARCH LETTERS, VOL. 33, L13306, doi:10.1029/2006GL025681, 2006

Unraveling the sequence of serpentinization reactions: petrography, mineral chemistry, and petrophysics of serpentinites from MAR 15°N (ODP Leg 209, Site 1274)

Wolfgang Bach,[1,2] Holger Paulick,[3] Carlos J. Garrido,[4] Benoit Ildefonse,[5] William P. Meurer,[6] and Susan E. Humphris[7]

Received 9 January 2006; revised 17 March 2006; accepted 17 April 2006; published 6 July 2006.

[1] The results of detailed textural, mineral chemical, and petrophysical studies shed new light on the poorly constrained fluid-rock reaction pathways during retrograde serpentinization at mid-ocean ridges. Uniformly depleted harzburgites and dunites from the Mid-Atlantic Ridge at 15°N show variable extents of static serpentinization. They reveal a simple sequence of reactions: serpentinization of olivine and development of a typical mesh texture with serpentine-brucite mesh rims, followed by replacement of olivine mesh centers by serpentine and brucite. The serpentine mesh rims on relic olivine are devoid of magnetite. Conversely, domains in the rock that are completely serpentinized show abundant magnetite. We propose that low-fluid-flux serpentinization of olivine to serpentine and ferroan brucite is followed by later stages of serpentinization under more open-system conditions and formation of magnetite by the breakdown of ferroan brucite. Modeling of this sequence of reactions can account for covariations in magnetic susceptibility and grain density of the rocks. **Citation:** Bach, W., H. Paulick, C. J. Garrido, B. Ildefonse, W. P. Meurer, and S. E. Humphris (2006), Unraveling the sequence of serpentinization reactions: petrography, mineral chemistry, and petrophysics of serpentinites from MAR 15°N (ODP Leg 209, Site 1274), *Geophys. Res. Lett.*, *33*, L13306, doi:10.1029/2006GL025681.

1. Introduction

[2] Serpentinization of ultramafic rocks at mid-ocean ridges profoundly influences rheology [e.g., *Escartín et al.*, 1997], magnetic anomalies [*Dyment et al.*, 1997], gravity, and seismic structure [e.g., *Mével*, 2003] of the oceanic lithosphere. Serpentinite-hosted vent fields appear to be common along slow and ultraslow spreading ridges [*Bach et al.*, 2002; *Baker et al.*, 2004]. Hydrogen and methane released during peridotite-seawater interactions [*Kelley et al.*, 2001; *Charlou et al.*, 2002] support microbial communities that form the base of the food web of unique ecosystems associated with serpentinite-hosted hydrothermal systems [*Kelley et al.*, 2005]. A number of recent microscopic [*Dodony and Buseck*, 2004], experimental [*Allen and Seyfried*, 2003], and theoretical studies [*Wetzel and Shock*, 2000; *Sleep et al.*, 2004] have addressed the geochemical and mineralogical transformations associated with serpentinization of abyssal peridotite [cf. *Evans*, 2004; *Früh-Green et al.*, 2004; *Mével*, 2003; *Schroeder et al.*, 2002].

[3] Despite this renewed interest in serpentinization of the seafloor, the underlying peridotite-water reactions are poorly constrained. In many cases, serpentinization is regarded as a single-step hydration of olivine to serpentine, brucite, and magnetite with release of H_2.

[4] We have investigated the textural and mineral chemical evolution of retrograde serpentinization of harzburgite and dunite drilled during Ocean Drilling Program Leg 209 at Site 1274 on the Mid-Atlantic Ridge (MAR) 15°39′N. In this paper, we describe this evolution and examine Fe partitioning among magnetite, brucite, and silicates during progressive retrograde serpentinization. We then propose a sequence of serpentinization reactions that reconciles petrographic observations with mass balance and physical properties (density and magnetic susceptibility) constraints.

2. Geological Setting

[5] The area of the 15°20′N Fracture Zone on the Mid-Atlantic Ridge has long been known for exposures of serpentinite and the presence of hydrothermal systems [*Rona et al.*, 1987]. Recent studies [*Escartín and Cannat*, 1999; *Fujiwara et al.*, 2003] have further constrained the extent of peridotite exposure and hydrothermal activity in the area. Close to the fracture zone, oblique faults and extensive outcrops of serpentinized peridotite are common, suggesting a heterogeneous lithosphere [*Escartín and Cannat*, 1999]. Enhanced fracturing and serpentinization of the lithosphere takes place in the vicinity of the transform fault. Serpentinization likely continues during uplift and exhumation of the serpentinized lithosphere on the rift valley walls [*Bach et al.*, 2004].

[6] Site 1274 is located 31 km north of the 15°20′N Fracture Zone on the western rift valley wall at 3940 m depth and approximately 700 m west of the termination of the detachment fault [*Kelemen et al.*, 2004]. Hole 1274A is 155.8 m deep and recovered 34.7 m of serpentinized harzburgite and dunite cut by serpentine fault gouge and

[1]Department of Marine Chemistry and Geochemistry, Woods Hole Oceanographic Institution, Woods Hole, Massachusetts, USA.
[2]Now at Geoscience Department, University of Bremen, Bremen, Germany.
[3]Mineralogisch-Petrologisches Institut, Universität Bonn, Bonn, Germany.
[4]Departamento de Mineralogia y Petrologia Facultad de Ciencias, Fuentenueva s/n Universidad de Granada, Granada, Spain.
[5]Laboratoire de Tectonophysique, ISTEEM (CNRS-UM2), Université Montpellier II, Montpellier, France.
[6]Department of Geosciences, University of Houston, Houston, Texas, USA.
[7]Department of Geology and Geophysics, Woods Hole Oceanographic Institution, Woods Hole, Massachusetts, USA.

0094-8276/06/2006GL025681$05.00

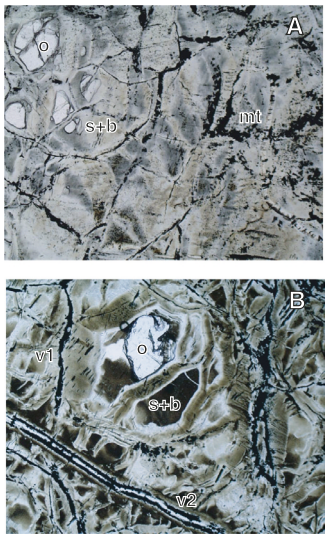

Figure 1. Thin section photomicrographs (parallel nicols) of serpentinites from Hole 1274A. The field of view is 1.7 mm wide. (a) Relic mesh center olivine (o) in the upper left corner, magnetite-free mesh rims (s + b), and magnetite accumulations (mt) in veins and completely serpentinized patches (Sample 1274A-17R-1, 121–129 cm). (b) Replacement of mesh center olivine (o) by serpentine + brucite (s + b). Magnetite veins (v1) are cut by later serpentine-magnetite veins (v2) (Sample 1274A-20R-1, 121–126 cm).

scarce dikes of rodingitized gabbro. The extent of serpentinization increases downhole from 60–70% near the seafloor to 95–100% at 70 meters below seafloor (mbsf). Serpentinization is nearly complete in the interval of abundant fault gouge between 70 and 140 mbsf, and then decreases to 85–90% near the bottom of the hole. Mass balance calculations indicate that serpentinization was isochemical except for the addition of water [*Paulick et al.*, 2006].

[7] The vertical variation in the intensity of serpentinization is mirrored by corresponding variations in physical properties. Magnetic susceptibility is relatively low at the top of the hole, increases gradually reaching highs of 0.1 SI near 110 mbsf, and then decreases toward the bottom of the hole. In contrast, densities decrease to a low of 2500 kg/m^3 where serpentinization is complete [*Shipboard Science Party*, 2004].

3. Petrography

[8] Thin-section petrography of variably serpentinized harzburgite and dunite from Hole 1274A reveals a simple sequence of reactions. Serpentinization of olivine and development of a typical mesh texture with serpentine mesh rims (Figure 1a) was followed by replacement of olivine mesh centers by serpentine and brucite (Figure 1b). Brucite was confirmed by whole rock X-ray diffraction work, and reconnaissance microchemical analyses by transmission electron microscopy (at University of Granada) showed the presence of nanometer-scale intergrowth of ferroan brucite and lizardite in mesh rims. Similar occurrences of brucite have been documented in samples from the Oman ophiolite [*Baronnet and Boudier*, 2001].

[9] The serpentine mesh rims on relic olivine are devoid of magnetite (Figure 1a). However, domains in the rock that are completely serpentinized show abundant magnetite, either in stringers or patches (Figure 1a) or in late magnetite and serpentine+magnetite veins (Figure 1b). Orthopyroxene was replaced, and commonly pseudomorphed (bastite), by serpentine. Talc and tremolite after orthopyroxene are not developed. Serpentinization took place under static conditions as indicated by the lack of interpenetrating textures. The compositions of serpentinized olivine and orthopyroxene are plotted in a FeO-SiO_2-MgO ternary in Figure 2. Electron microprobe analyses of olivine and orthopyroxene indicate that both phases have Mg-numbers (molar Mg/(Mg + Fe) $\times$ 100) of around 90. The compositions of the mesh rims on relic olivine (Figure 2) indicate that the initial serpentinization of olivine produced magnesian serpentine (Mg#95). A large number of mesh rim analyses plot along a trend that connects olivine and serpentine compositions and extends toward brucite with Mg#75. This trend, in addition to the conspicuous lack of magnetite in the mesh rims, indicates that Fe partitions primarily into brucite, and also suggests that the initial serpentinization of olivine was quasi-isochemical. In contrast, later replacement of olivine mesh centers by serpentine (Mg#95) and with magnesian brucite (Mg#90) was associated with a loss of Fe relative to Mg. During the serpentinization of orthopyroxene, the Mg/Fe ratio appears to be preserved; that is, En_{90} orthopyroxene is replaced by Mg#90 serpentine (Figure 2).

4. Serpentinization Reactions

[10] Based on these textural and compositional relationships, we propose the following sequence of serpentiniza-

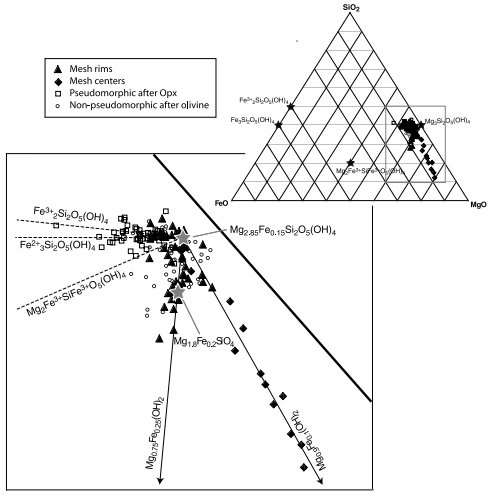

Figure 2. FeO-SiO_2-MgO (molar proportions) ternary plot of serpentine (+brucite) compositions from Hole 1274A [after *Wicks and Plant*, 1979]. Inset shows the entire ternary with endmember serpentine compositions marked by stars. The box indicates the enlarged area. Tie lines extend to hypothetical serpentine endmembers. The mesh rims plot along a line that connects serpentine (Mg#95) with brucite (Mg#75). The mesh centers indicate a more magnesian (Mg#90) brucite composition and generally higher brucite proportions. Electron microprobe analyses were conducted at the Universities of Bonn and Houston, using 15 kV acceleration voltage, 10 nA beam current, and a beam diameter of 5 μm.

tion reactions: Isochemical reaction of olivine (Mg#90) to serpentine (Mg#95) and Fe-rich brucite (Mg#75):

$$2\ Mg_{1.8}Fe_{0.2}SiO_4 + 3\ H_2O = 1\ Mg_{2.85}Fe_{0.15}Si_2O_5(OH)_4 + 1\ Mg_{0.75}Fe_{0.25}(OH)_2 \quad \text{(R1)}$$

Reaction of Fe-rich brucite with aqueous silica to form serpentine and magnetite:

$$57\ Mg_{0.75}Fe_{0.25}(OH)_2 + 30\ SiO_2(aq) = 15\ Mg_{2.85}Fe_{0.15}Si_2O_5(OH)_4 + 23\ H_2O + 4\ Fe_3O_4 + 4\ H_2 \quad \text{(R2)}$$

The source of the aqueous silica for reaction (2) is likely provided by the breakdown of orthopyroxene to serpentine:

$$3\ Mg_{0.9}Fe_{0.1}SiO_3 + 2\ H_2O = Mg_{2.7}Fe_{0.3}Si_2O_5(OH)_4 + SiO_2(aq) \quad \text{(R3)}$$

This reaction becomes more important in controlling the composition of the interacting fluid as serpentinization progresses and olivine nears exhaustion.

5. Magnetic Susceptibility–Density Relationships

[11] The bulk magnetic susceptibility of whole rock samples from Hole 1274A that are between 70 and 100% serpentinized increases exponentially as grain density decreases (Figure 3). We have used the method introduced by *Toft et al.* [1990] to calculate how these physical properties would change with increasing serpentinization for different types of serpentization reactions. Our calculations confirm the finding by *Toft et al.* [1990] that no single-step reaction of olivine to serpentine, brucite, and magnetite can explain this relationship (Figure 3, dashed line).

[12] We now test if our proposed model of serpentinization can explain the observed variations in density and magnetic susceptibility. The solid line shows results for a model that assumes reaction (1) dominates in the early stages of serpentinization, while reaction (2) becomes increasingly important during later serpentinization stages. Consistent with petrographic observations, we assume that the initial serpentinization (up to 40 Mol.% of the serpentinization) is exclusively by reaction (1), while reaction (2) becomes increasingly important with progressive serpentinization. In the model, we let reaction (1) proceed at a constant pace of 0.1 mole serpentine produced per incremental step. Reaction (2) is first allowed in step 5, with an assigned step number 1 and an initial step size that is 0.1% of that for reaction (1) (i.e., 0.0001 mole serpentine and magnetite per incremental step). The rate of reaction (2) was then increased relative to that of reaction (1) following a simple power-law that has the step number multiplied by 0.0001 as base number and an arbitrary number as power. The best fit (Figure 3) was found for a power of 3.

6. Discussion and Conclusions

[13] The production of magnetite during serpentinization has huge implications for rock magnetic properties, including the possible contribution of serpentinite to oceanic magnetic anomalies. In addition to finding that a single-step reaction of primary Mg-Fe silicates to serpentine and magnetite (±brucite) cannot explain the exponential increase in magnetic susceptibility with decreasing rock density, *Toft et al.* [1990] proposed a reaction sequence that invokes intermediary Fe-rich serpentinite and brucite. Consistent with this suggestion, *Oufi et al.* [2002] found that the Fe content of serpentine decreases and the amount of secondary magnetite increases with progressive serpentinization. They concluded that natural remanent magnetizations similar to those of fresh basalt are not produced until 75% of the peridotite is serpentinized.

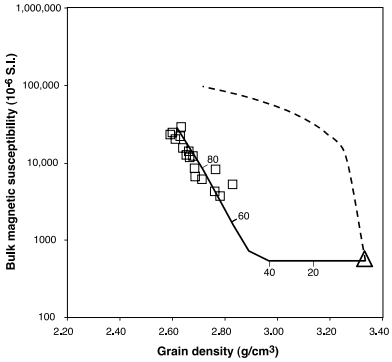

Figure 3. Relation between bulk magnetic susceptibility and grain density for Hole 1274A whole rock samples that are between 70 and 100% serpentinized [*Shipboard Science Party*, 2004]. The triangle represents a typical fresh peridotite. Trend lines were calculated following the procedures of *Toft et al.* [1990]. The dashed line is calculated for a single-step reaction of olivine (Fo90) and water to Mg-serpentine, Mg-brucite, magnetite, and hydrogen [cf. *Toft et al.*, 1990, reaction 15]. The solid line represents results of a two-step model. Marks and labels refer to the Mol% of serpentine formed according to reaction (1). See text for more detailed explanation.

[14] Our results are consistent with the idea that magnetite formation peaks when >60–70% of the peridotite is serpentinized. We propose that the evolution of textural, mineral chemical and bulk physical properties during serpentinization is a consequence of a sequence of serpentinization reactions that start with low fluid flux (quasi-isochemical) serpentinization of olivine to serpentine and ferroan brucite. Later-stage serpentinization is more open-system and results in formation of magnetite, primarily from the breakdown of ferroan brucite. Magnetite formation by this mechanism requires high silica activities and may be inhibited initially as the composition of the interacting fluid is controlled by the reaction of olivine. When the olivine is nearly exhausted (60–75% serpentinization of harzburgite), the interacting fluids are expected to be more strongly influenced by the reaction of orthopyroxene. This results in higher SiO_2(aq) activities, which facilitates the reaction of ferroan brucite to serpentine and magnetite. The replacement of relic olivine cores by serpentine and magnesian brucite likely takes place after the main-stage serpentinization.

[15] Coupled to the formation of magnetite is the production of hydrogen that is a key component in setting

the chemical compositions of serpentinization fluids and supporting microbial habitats in serpentinite-hosted hydrothermal systems. *Sleep et al.* [2004] suggested that serpentine(Mg#90)-brucite-magnetite equilibria will reach supersaturation levels of hydrogen over a temperature range of 160° to 350°C at 500 bars. A mass balance of reactions (1)–(3) indicates that 28.5 moles of olivine (4.2 kg) may produce 1 mole of H_2. At a water-to-rock mass ratio of 1, this corresponds to ~250 mM H_2, which is below the solubility of H_2(aq) (~1.4M at 300°C and 500 bars) but higher than H_2(aq) concentrations measured in vent fluids from axial serpentinite-hosted systems (12–16 mM [*Charlou et al.*, 2002]).

[16] Finally, we acknowledge that the reaction pathways proposed in this paper are not representative for all serpentinization systems. In fact, vent fluid compositions [*Kelley et al.*, 2001; *Mottl et al.*, 2003; *Charlou et al.*, 2002] suggest that there is a strong variability in pH, aH_2(aq), $aSiO_2$(aq), etc. that must reflect differences in the conditions of water-peridotite interactions. Improving our ability to use the rock record in reconstructing serpentinization reactions, and increasing the predictive strength of geochemical reaction models, will be required to further our understanding of the role of serpentinization in terrestrial and deep-sea serpentinite-hosted geochemical and microbiological systems of the modern and ancient Earth.

[17] **Acknowledgments.** This research used data and/or samples supplied by the Ocean Drilling Program (ODP). ODP is sponsored by the U.S. National Science Foundation (NSF) and participating countries under management of Joint Oceanographic Institutions (JOI), Inc. We thank two anonymous reviewers for helpful comments, Jeff Seewald, Ron Frost, and Tom McCollom for useful discussions, and Bernhard Evans for a critical review of an earlier version of the paper. Funding for this research was provided by USSSP and NSF-OCE grant 9986135. WB acknowledges support through a fellowship by the Deep Ocean Exploration Institute.

References

Allen, D. E., and W. E. J. Seyfried (2003), Compositional controls on vent fluids from ultramafic-hosted hydrothermal systems at mid-ocean ridges: An experimental study at 400°C, 500 bars, *Geochim. Cosmochim. Acta*, *67*, 1531–1542.

Bach, W., N. R. Banerjee, H. J. B. Dick, and E. T. Baker (2002), Discovery of ancient and active hydrothermal systems along the ultra-slow spreading Southwest Indian Ridge 10°–16°E, *Geochem. Geophys. Geosyst.*, *3*(7), 1044, doi:10.1029/2001GC000279.

Bach, W., C. J. Garrido, H. Paulick, J. Harvey, and M. Rosner (2004), Seawater-peridotite interactions: First insights from ODP Leg 209, MAR 15°N, *Geochem. Geophys. Geosyst.*, *5*, Q09F26, doi:10.1029/2004GC000744.

Baker, E. T., H. N. Edmonds, P. J. Michael, W. Bach, H. J. B. Dick, J. E. Snow, S. L. Walker, N. R. Banerjee, and C. H. Langmuir (2004), Hydrothermal venting in magma deserts: The ultraslow-spreading Gakkel and Southwest Indian Ridges, *Geochem. Geophys. Geosyst.*, *5*, Q08002, doi:10.1029/2004GC000712.

Baronnet, A., and F. Boudier (2001), Microstructural and microchemical aspects of serpentinization, *Lunar Planet. Sci.* [CD-ROM], *XI*, Abstract 3382.

Charlou, J.-L., et al. (2002), Geochemistry of high H_2 and CH_4 vent fluids issuing from ultramafic rocks at the Rainbow hydrothermal field (36°14′N, MAR), *Chem. Geol.*, *191*, 345–359.

Dodony, I., and P. Buseck (2004), Serpentinites close-up and intimate: An HRTEM view, *Int. Geol. Rev.*, *46*, 507–527.

Dyment, J., et al. (1997), Contribution of serpentinized ultramafics to marine magnetic anomalies at slow and intermediate spreading centres: Insights from the shape of the anomalies, *Geophys. J. Int.*, *129*, 691–701.

Escartín, J., and M. Cannat (1999), Ultramafic exposures and the gravity signature of the lithosphere near the Fifteen-Twenty Fracture Zone (Mid-Atlantic Ridge, 14°–16.5°N), *Earth Planet. Sci. Lett.*, *171*, 411–424.

Escartín, J., et al. (1997), Effects of serpentinization on the lithospheric strength and the style of normal faulting at slow-spreading ridges, *Earth Planet. Sci. Lett.*, *151*, 181–189.

Evans, B. W. (2004), The serpentine multisystem revisited: Chrysotile is metastable, *Int. Geol. Rev.*, *46*, 479–506.

Früh-Green, G. L., et al. (2004), Serpentinization of oceanic peridotites: Implications for geochemical cycles and biological activity, in *The Subseafloor Biosphere at Mid-Ocean Ridges*, *Geophys. Monogr. Ser.*, vol. 144, edited by W. S. D. Wilcock et al., pp. 119–136, AGU, Washington, D. C.

Fujiwara, T., J. Lin, T. Matsumoto, P. B. Kelemen, B. E. Tucholke, and J. F. Casey (2003), Crustal Evolution of the Mid-Atlantic Ridge near the Fifteen-Twenty Fracture Zone in the last 5 Ma, *Geochem. Geophys. Geosyst.*, *4*(3), 1024, doi:10.1029/2002GC000364.

Kelemen, P., et al. (2004), ODP Leg 209 drills into mantle peridotite along the Mid-Atlantic Ridge from 14°N to 16°N, *JOIDES J.*, *30*, 14–20.

Kelley, D. S., et al. (2001), An off-axis hydrothermal vent field near the Mid-Atlantic Ridge at 30°N, *Nature*, *412*, 127–128.

Kelley, D. S., et al. (2005), A serpentinite-hosted ecosystem: The Lost City Hydrothermal Field, *Science*, *307*, 1428–1434.

Mével, C. (2003), Serpentinization of abyssal peridotite at mid-ocean ridges, *C. R. Geosci.*, *335*, 825–852.

Mottl, M. J., S. C. Komor, P. Fryer, and C. L. Moyer (2003), Deep-slab fluids fuel extremophilic Archaea on a Mariana forearc serpentinite mud volcano: Ocean Drilling Program Leg 195, *Geochem. Geophys. Geosyst.*, *4*(11), 9009, doi:10.1029/2003GC000588.

Oufi, O., M. Cannat, and H. Horen (2002), Magnetic properties of variably serpentinized abyssal peridotites, *J. Geophys. Res.*, *107*(B5), 2095, doi:10.1029/2001JB000549.

Paulick, H., W. Bach, M. Godard, C.-J. Hoog, G. Suhr, and J. Harvey (2006), Geochemistry of abyssal peridotites (Mid-Atlantic Ridge, 15°20′N, ODP Leg 209): Implications for fluid/rock interaction in slow spreading environments, *Chem. Geol.*, in press.

Rona, P. A., et al. (1987), Serpentinized ultramafics and hydrothermal activity at the Mid-Atlantic Ridge crest near 15°N, *J. Geophys. Res.*, *92*, 1417–1427.

Schroeder, T., et al. (2002), Geologic implications of seawater circulation through peridotite exposed at slow-spreading ridges, *Geology*, *30*, 367–370.

Shipboard Science Party (2004), Leg 209 summary, in *Proc. Ocean Drill. Program, Initial Rep.*, *209*, 1–139.

Sleep, N. H., et al. (2004), H_2-rich fluids from serpentinization: Geochemical and biotic implications, *Proc. Natl. Acad. Sci. U. S. A.*, *104*, 818–12,823.

Toft, P. B., et al. (1990), The effects of serpentinization on density and magnetic susceptibility: A petrophysical model, *Phys. Earth Planet. Inter.*, *65*, 137–157.

Wetzel, L. R., and E. L. Shock (2000), Distinguishing ultramafic- from basalt-hosted submarine hydrothermal systems by comparing calculated vent fluid compositions, *J. Geophys. Res.*, *105*, 8319–8340.

Wicks, F. J., and A. G. Plant (1979), Electron-microprobe and x-ray-microbeam studies of serpentine textures, *Can. Mineral.*, *17*, 785–830.

W. Bach, Geoscience Department, University of Bremen, Klagenfurter Str. 2, D-28359 Bremen, Germany. (wbach@uni-bremen.de)

C. J. Garrido, Departamento de Mineralogia y Petrologia Facultad de Ciencias, Fuentenueva s/n Universidad de Granada, E-18002 Granada, Spain. (carlosg@ugr.es)

S. E. Humphris, Department of Geology and Geophysics, Woods Hole Oceanographic Institution, 360 Woods Hole Road, Woods Hole, MA 02543, USA. (shumphris@whoi.edu)

B. Ildefonse, Laboratoire de Tectonophysique, ISTEEM (CNRS-UM2), cc 49 - Université Montpellier II, F-34095 Montpellier cedex 05, France. (benoit@dstu.univ-montp2.fr)

W. P. Meurer, Department of Geosciences, University of Houston, 312 Science and Research Bldg. 1, Houston, TX 77204–5007, USA. (wpmeurer@mail.uh.edu)

H. Paulick, Mineralogisch-Petrologisches Institut, Universität Bonn, Poppelsdorfer Schloss, D-53115 Bonn, Germany. (holger.paulick@uni-bonn.de)